LETTER

doi:10.1038/nature13397

Millennial-scale variability in Antarctic ice-sheet discharge during the last deglaciation

M. E. Weber[1], P. U. Clark[2], G. Kuhn[3], A. Timmermann[4], D. Sprenk[1], R. Gladstone[5], X. Zhang[3], G. Lohmann[3], L. Menviel[6,7], M. O. Chikamoto[4], T. Friedrich[4] & C. Ohlwein[8]

Our understanding of the deglacial evolution of the Antarctic Ice Sheet (AIS) following the Last Glacial Maximum (26,000–19,000 years ago)[1] is based largely on a few well-dated but temporally and geographically restricted terrestrial and shallow-marine sequences[2–4]. This sparseness limits our understanding of the dominant feedbacks between the AIS, Southern Hemisphere climate and global sea level. Marine records of iceberg-rafted debris (IBRD) provide a nearly continuous signal of ice-sheet dynamics and variability. IBRD records from the North Atlantic Ocean have been widely used to reconstruct variability in Northern Hemisphere ice sheets[5], but comparable records from the Southern Ocean of the AIS are lacking because of the low resolution and large dating uncertainties in existing sediment cores. Here we present two well-dated, high-resolution IBRD records that capture a spatially integrated signal of AIS variability during the last deglaciation. We document eight events of increased iceberg flux from various parts of the AIS between 20,000 and 9,000 years ago, in marked contrast to previous scenarios which identified the main AIS retreat as occurring after meltwater pulse 1A[3,6–8] and continuing into the late Holocene epoch. The highest IBRD flux occurred 14,600 years ago, providing the first direct evidence for an Antarctic contribution to meltwater pulse 1A. Climate model simulations with AIS freshwater forcing identify a positive feedback between poleward transport of Circumpolar Deep Water, subsurface warming and AIS melt, suggesting that small perturbations to the ice sheet can be substantially enhanced, providing a possible mechanism for rapid sea-level rise.

Today, the estimated total iceberg calving flux from Antarctica is about 1,300–2,000 gigatons per year (Gt yr^{-1})[9], with giant (longer than 18 km) icebergs representing at least half of the total AIS mass loss[10]. Iceberg trajectory studies for the sea-ice-covered part of the Southern Ocean show that only a small fraction of icebergs calving from the AIS escapes coastal regions directly to the north, owing to topographic steering of ocean currents[9]. Otherwise, a substantial fraction of large icebergs[9] remain entrained in the westward-flowing Antarctic Coastal Current, travelling counter-clockwise around Antarctica before entering the Weddell Sea[11] (Fig. 1). Here, they follow the cyclonic wind-driven Weddell Gyre, where they merge with icebergs calving from the Filchner–Rønne Ice Shelf in the southern Weddell Sea. These icebergs then travel north through the so-called 'Iceberg Alley' and exit the Weddell Sea basin to

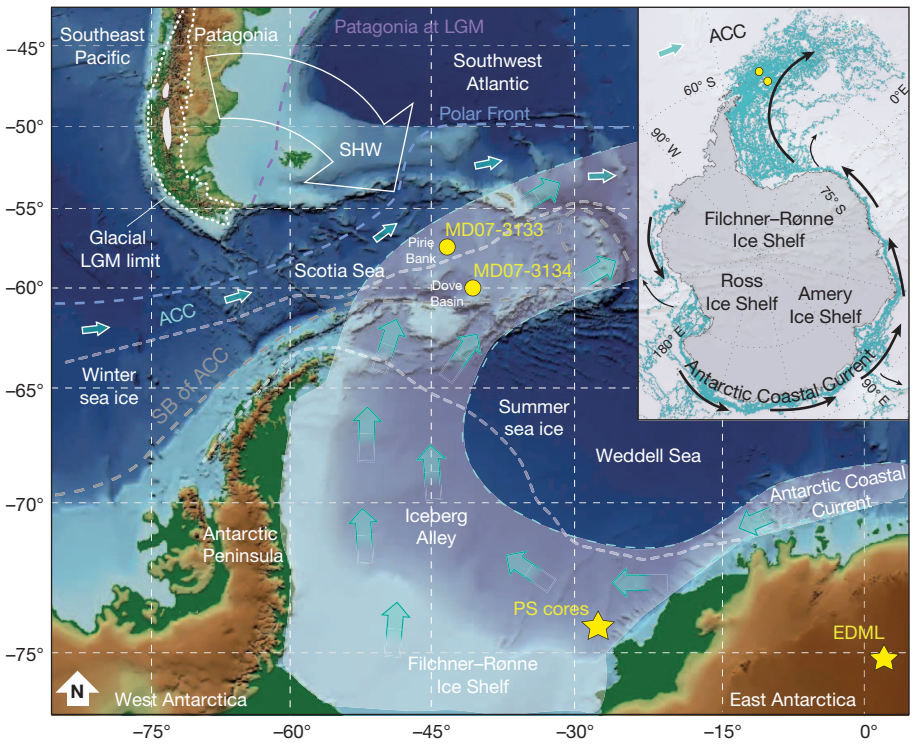

Figure 1 | Location map. Sites MD07-3133 and MD07-3134 are located in the central Scotia Sea. Open arrows refer to Iceberg Alley. The large grey arrow indicates the Southern Hemisphere westerly winds (SHW). The southern boundary of the Antarctic Circumpolar Current (SB of ACC) is indicated by a grey dashed line. White dashed lines describe winter and summer sea-ice extent. Research vessel Polarstern (PS) cores refer to ice-sheet retreat studies conducted in the southeastern Weddell Sea[4]. The inset map (upper right) shows the circum-Antarctic drift of icebergs (turquoise; ≥5 km in length) calving off the Antarctic ice shelves from 1999 to 2009 (ref. 11). Black arrows indicate the general counterclockwise flow within the Antarctic Coastal Current.

[1]Institute of Geology and Mineralogy, University of Cologne, Zuelpicher Strasse 49a, 50935 Cologne, Germany. [2]College of Earth, Ocean, and Atmospheric Sciences, Oregon State University, Corvallis, Oregon 97331, USA. [3]Alfred-Wegener-Institut Helmholtz-Zentrum für Polar- und Meeresforschung, Am Alten Hafen 26, 27568 Bremerhaven, Germany. [4]International Pacific Research Center, School of Ocean and Earth Sciences and Technology, University of Hawaii at Manoa, 2525 Correa Road, Honolulu, Hawaii 96822, USA. [5]Arctic Centre, University of Lapland, PO Box 122, 96101 Rovaniemi, Finland. [6]Climate Change Research Centre, Level 4, Mathews Building, University of New South Wales, Sydney, New South Wales 2052, Australia. [7]ARC Centre of Excellence for Climate System Science, University of New South Wales, Sydney, New South Wales 2052, Australia. [8]Hans-Ertel Centre for Weather Research/Climate Monitoring Branch, Meteorological Institute, University of Bonn, Auf dem Hügel 20, 53121 Bonn, Germany.

the northeast into the Scotia Sea (Fig. 1). Around 55° S–60 °S, icebergs start to move in a more eastward direction as they are swept into the warmer Antarctic Circumpolar Current. Melt rates remain low until the warmer Antarctic Circumpolar Current is reached, after which the icebergs ablate rapidly in the general area of our core sites.

We present two high-resolution records of IBRD from deep-sea core sites MD07-3133 and MD07-3134, collected from the south-central Scotia Sea (Fig. 1) (Methods). Dating relies mainly on the correlation of dust records from our cores to the Antarctic European Project for Ice Coring in Antarctica (EPICA) Dronning Maud Land (EDML) dust record[12] (Methods). Ages reported here refer to the EDML1 or EPICA Dome C (EDC) 3 age scale (Methods). The cores are located in the centre of Iceberg Alley, the primary route taken by large icebergs from the AIS that remained entrained in the Antarctic Coastal Current today as well as during the last deglaciation (Methods). Owing to the loss of some icebergs northwards from the Antarctic Coastal Current, and the gradual ablation of icebergs within the Antarctic Coastal Current, relatively fewer icebergs may reach our sites from more distant sources (Methods). Although the primary IBRD content of icebergs may vary substantially and most of the coarser basal material is released close to the source (that is, the coarse-grained IBRD signal may have a regional bias towards the Weddell Sea and the Antarctic Peninsula), the majority of the fine-grained englacial material determined here should capture a spatially more integrated signal that is representative of variability in the flux of icebergs released by the AIS (except for the Amundsen Sector), particularly in a colder climate than today's.

The IBRD record from site MD07-3134 exhibits a number of peaks starting at about 20,000 years (20 kyr) ago and continuing through the deglaciation until about 9 kyr ago, when modern IBRD levels were reached (Fig. 2c). Most of the pronounced IBRD events are replicated at site MD07-3133 (Fig. 2d), which is about 300 km to the northwest (Fig. 1), thus providing a robust signal of episodic enhanced iceberg flux through Iceberg Alley. Stacking the IBRD records (Fig. 2e) and their fluxes (Fig. 2f) (Methods) identifies eight primary episodes of enhanced iceberg flux originating from different parts of the AIS that began within one to several decades and lasted from centuries to a millennium. These records thus provide the first evidence for substantial centennial to millennial variability in mass loss from the AIS throughout much of the last deglaciation. We refer to these events as Antarctic Ice Sheet discharges (AID8 to AID1, from oldest to youngest); for error estimates on the timing and duration of AIDs see Methods.

AID8 occurred 20–19 kyr ago (Fig. 2), which corresponds to the start of the deglaciation of the Antarctic Peninsula Ice Sheet[2] and the East AIS in the southeastern Weddell Sea[4]. Although the IBRD event in the stacked record has a concentration of debris similar to that of several of the younger events, its flux (Fig. 2f) is the smallest, which is consistent with an early onset of deglaciation for just the Antarctic Peninsula and Weddell Sea sectors in response to increasing Southern Hemisphere obliquity and sea-level forcing originating from the onset of deglaciation of Northern Hemisphere ice sheets[4].

Subsequent AID events generally have similar or larger concentration in the IBRD stack than does AID8 (Fig. 2e), whereas the IBRD fluxes of AID7 to AID1 exceed those of AID8 (Fig. 2f). AID7 started 17 kyr ago, with IBRD increasing until around 15.7 kyr ago, when the event abruptly ended. The distinct IBRD peak near the end of AID7 about 16 kyr ago has been documented as a second retreat phase of the Weddell Sea sector of the East AIS[4]. Moreover, most of the marine-based sectors of the Antarctic Peninsula Ice Sheet had retreated by about 16.7 kyr ago[2], along

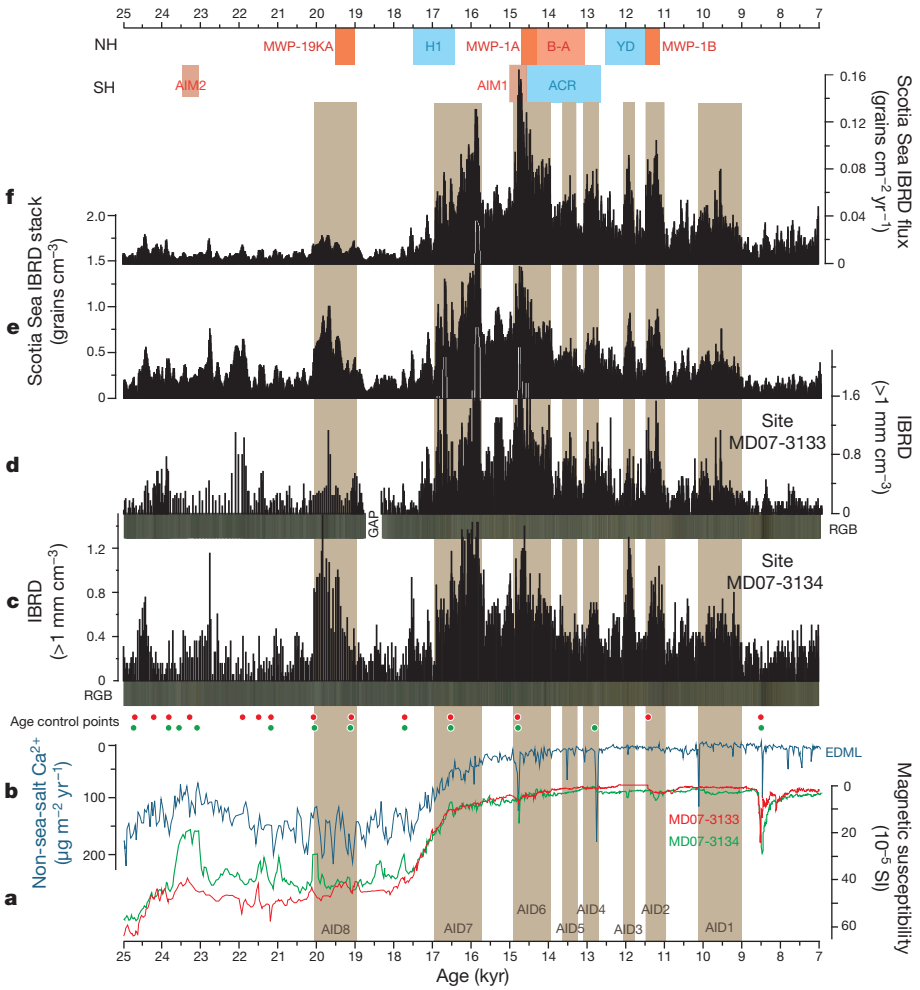

Figure 2 | Climate development from the Last Glacial Maximum to the Holocene (25–7 kyr ago). Eight phases of enhanced iceberg flux through Iceberg Alley were detected and named AID1 to AID8. **a**, Magnetic susceptibility (in SI units) record of sites MD07-3133 and MD07-3134 (ref. 12). **b**, EDML ice-core non-sea-salt Ca flux on the EDML1/EDC3 timescale[27]. **c**, IBRD with red, green, blue (RGB) colour log for site MD07-3134 and site MD07-3133 (**d**). **e**, Stacked IBRD record. **f**, Stacked IBRD flux record (Methods). AID8–AID1 occurred at approximately 20–19 kyr ago, 17–16 kyr ago, 15–14 kyr ago, 13.5 kyr ago, 13 kyr ago, 12 kyr ago, 11 kyr ago and 10–9 kyr ago. The top panel identifies Northern Hemisphere (NH) climate signals MWP-19KA, Heinrich event 1 (H1), MWP-1A, Bølling–Allerød (B–A), Younger Dryas (YD), and MWP-1B, as well as Southern Hemisphere (SH) Antarctic Isotopic Maxima (AIM) 2 and 1, and the Antarctic Cold Reversal (ACR).

with sectors of the West AIS (for example, the Pine Island glacier of the Amundsen Sea embayment) at 16.4 kyr ago (Methods) that are generally coincident with the major increase in the Scotia Sea IBRD flux rates starting at 16.4 kyr ago (Fig. 2f).

The start of AID7 follows the onset of Antarctic-wide deglacial warming[13] (Fig. 3f) and the retreat of sea ice[13] (Fig. 3e). As indicated by a decrease in the stable carbon isotope ratio of atmospheric carbon $\delta^{13}C_{atm}$ (ref. 14; Fig. 3c), enhanced Southern Ocean opal flux (Fig. 3d), and declining dust/magnetic susceptibility contents (Fig. 2a,b), the onset of AID7 is accompanied by enhanced Southern Ocean ventilation and changes in atmospheric circulation that may have caused an encroachment of warmer water to the AIS marine margins, leading to destabilization and a period of enhanced iceberg release.

There is a distinct pause in ice rafting between AID7 and AID6 (Figs 2, 3) accompanied by a slowdown in atmospheric warming in the Atlantic sector. The subsequent AID6 exhibits the largest IBRD flux (Fig. 3a and b). AID6 has a relatively abrupt onset at about 15 kyr ago and reaches its peak values approximately 14.8–14.4 kyr ago, followed by a more gradual decline until 13.9 kyr ago, when it abruptly ends. There is general agreement among the few existing well-dated records from Antarctica for widespread retreat of the AIS at this time, including from Mac Robertson Land of the East AIS, the Ross Sea sector of the West AIS, and the Antarctic Peninsula Ice Sheet[2,3] (Methods).

The interval of peak IBRD flux during AID6 (14.8–14.4 kyr ago ± 0.25 kyr, where the error is 1σ) is synchronous with the onset of the Bølling interstadial in the Northern Hemisphere (14.64 ± 0.09 kyr ago) (Fig. 3g) and with the period of rapid sea-level rise referred to as meltwater pulse (MWP) 1A (occurring 14.65–14.3 kyr ago ± 0.03 kyr ago)[15]. Fingerprinting studies using the new Tahiti sea-level record and other far-field records[15] support previous such studies[16] in identifying a substantial (at least 50%) Antarctic contribution to the global mean sea-level rise of about 14 m during MWP-1A. The fact that the peak flux of AID6 in our well-dated IBRD record is the same age and duration (around 400 years) as MWP-1A (as defined from the Tahiti record) provides direct evidence for an Antarctic contribution.

Several factors may have preconditioned or triggered the initial AIS grounding-line (boundary between the floating ice shelf and the grounded ice that rests on bedrock) retreat during AID6, including sea-level rise from melting of Northern Hemisphere ice sheets[17], subsurface warming associated with changes of the Atlantic Meridional Overturning Circulation[4], and increases of atmospheric greenhouse gas concentrations. To further explain the climate response to the meltwater discharge associated with AID6, we conducted a series of transient numerical modelling experiments with three different Earth system models (Methods). Assuming that AID6 freshwater forcing corresponded to a maximum sea-level rise of 20 mm yr^{-1} (50% of the maximum MWP-1A rate[15]), our model results show considerable Southern Ocean surface cooling, expansion of sea ice, formation of a halocline, reduction of Antarctic Bottom Water formation and subsurface warming at depths of 100–1,500 m through poleward migration of Circumpolar Deep Water (Fig. 4). Consistent with previous modelling experiments[18,19], we suggest that this ocean thermal forcing accelerated thinning of ice shelves by basal melting, inducing a positive feedback by causing grounding-line retreat, calving and subsequent release of more fresh water.

The next five IBRD events (AID5–AID2), which are of comparable concentration and duration, show a pacing with a repeat time of about 800–900 years. AID2 has the largest IBRD flux of these five events, attaining its peak flux at about 11.3 kyr ago, which corresponds to the age of MWP-1B recorded in the Barbados sea-level record[20]. The absence of an equivalent sea-level event in the Tahiti coral record[21] might reflect different far-field sea-level responses to a deglaciation event from the Pacific sector of the AIS[21]. Although our IBRD record does not distinguish

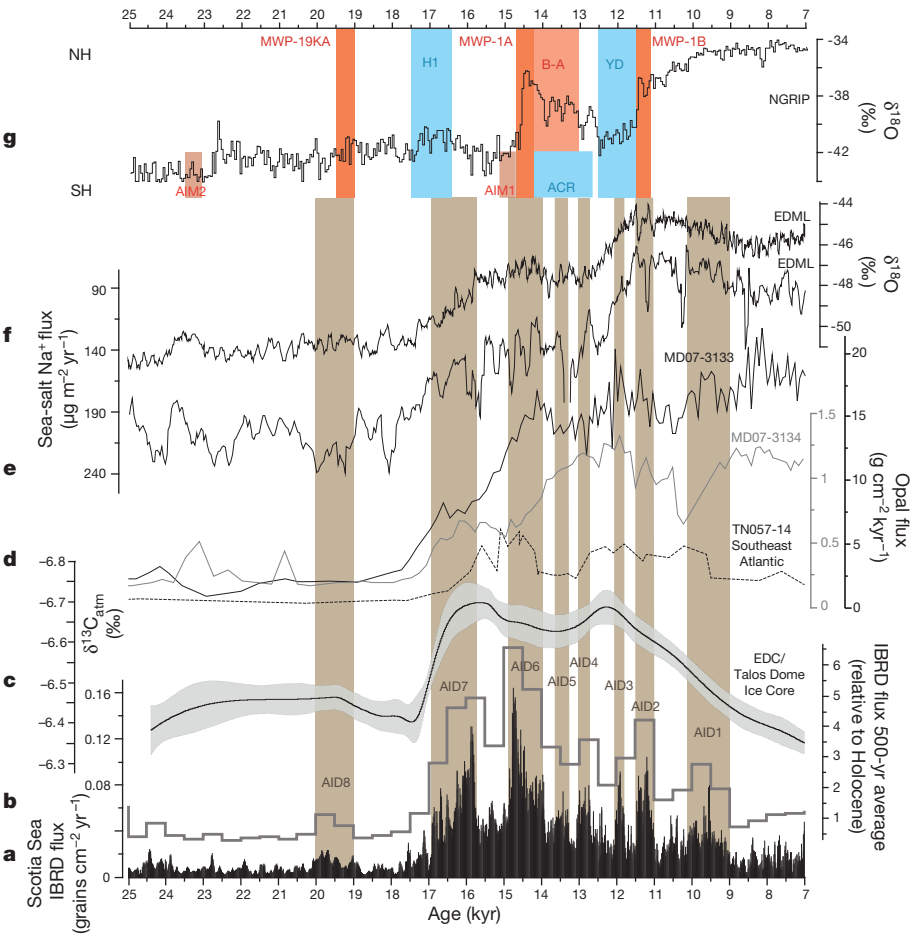

Figure 3 | IBRD flux in the Scotia Sea compared to climate changes during the last deglaciation. **a**, Stacked IBRD flux record. **b**, 500-yr averages of stacked IBRD flux relative to Holocene average (Methods). **c**, Antarctic deglacial $\delta^{13}C_{atm}$ stack with 1σ error (shaded)[14]. **d**, Biogenic opal flux records from the southeast Atlantic site TN057-14 (dashed)[28] and the Scotia Sea sites MD07-3133 (black) and MD07-3134 (grey)[29]. **e**, EDML ice-core record of sea-salt Na^+ flux[13]. **f**, $\delta^{18}O$ record from EDML ice core[13]. **g**, $\delta^{18}O$ record from NGRIP ice core[30]. Note that MWP-1A is coeval with AID6, within the dating uncertainties. Note further that major changes in the Southern Hemisphere commenced around 17 kyr ago when the Northern Hemisphere was cold during Heinrich event 1.

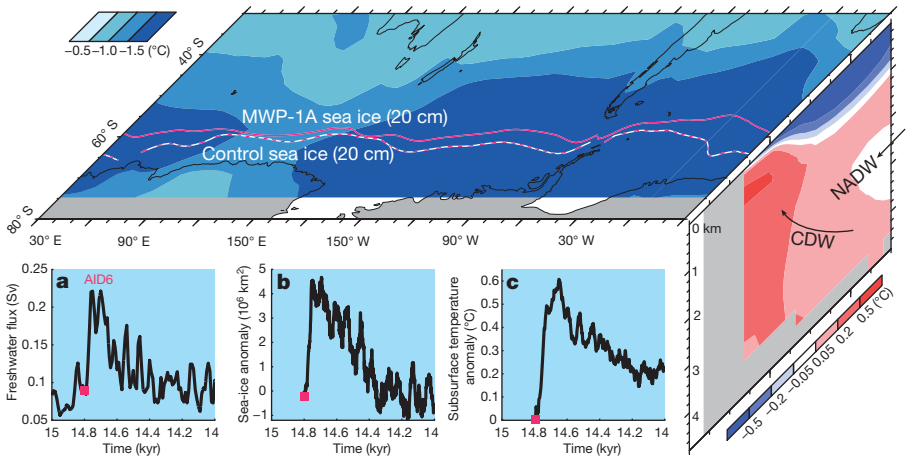

Figure 4 | Three-dimensional pattern of temperature anomalies at 14.8–14 kyr ago (AID6). The map shows mean surface air temperature anomaly; the vertical profile indicates zonally averaged ocean temperature anomaly in response to an Antarctic meltwater pulse of about 0.22 Sv at around 14.6 kyr ago. The multi-model mean is calculated by averaging the respective anomalies obtained from the Bern3D, LOVECLIM and COSMOS models (Methods). White-and-purple dashed and purple solid lines show the annual mean extent of 20-cm-thick sea ice for 14.8 kyr ago and 14.6 kyr ago, respectively, simulated by the LOVECLIM model. Note that freshwater forcing (**a**) causes surface cooling, an increase in zonally averaged sea-ice extent (**b**) and averaged subsurface warming between 800 m and 1,200 m and 63 °S and 70 °S (**c**). NADW, North Atlantic Deep Water; CDW, Circumpolar Deep Water.

the source of mass loss from the AIS, the presence of AID2 is consistent with an Antarctic contribution to MWP-1B as well[21].

The youngest IBRD event (AID1) started about 10 kyr ago, with the peak flux occurring around 9.5 kyr ago; it ended about 9 kyr ago. The only other available records that span this time are from the Ross Sea sector of the Western AIS, but they suggest that retreat of the grounding line in the Ross Sea occurred either before or after AID1. The specific sector of the AIS that contributed to this event thus remains unknown (Methods).

Our IBRD record shows clear evidence for episodic mass loss of the AIS during the last deglaciation, but further work is required to identify the sources of mass loss associated with each AID (Methods). Millennial-scale AIDs, similar to those observed in the Northern Hemisphere[5], are indicative of abrupt ice-sheet instabilities[22] that initiated within one to a few decades, released fresh water into the Southern Ocean, and contributed to the overall deglacial sea-level rise. The peak of AID6 is synchronous, within the dating uncertainties, with MWP-1A. Modelling results indicate that ocean thermal forcing from the transport of warm Circumpolar Deep Water to the base of ice shelves may have been an important positive feedback in AIS deglacial dynamics. Highlighting the role of ocean thermal forcing and rapid ice-sheet responses, our study provides an important palaeoclimate context for contemporaneous[23,24] and future[25,26] interactions between the ice sheet and the ocean around Antarctica.

METHODS SUMMARY

Chronology. Age models for cores MD07-3133 and MD07-3134 (ref. 12) were established by correlating their magnetic susceptibility signal, as well as the Ca and Fe records of MD07-3134, both of which largely reflect dust deposition in the circum-Antarctic region, to the dust (non-sea-salt Ca) flux record of the EDML ice core[27]. We assume that sediment-core magnetic susceptibility, Fe, Ca and ice-core non-sea-salt Ca are in phase because all signals are atmospheric, and therefore essentially reached marine and ice-sheet deposition sites synchronously. Sites MD07-3133 and MD07-3134 have average sedimentation rates of 92 cm kyr^{-1} and 63 cm kyr^{-1} over the last 36 kyr and 93 kyr, respectively, yielding a deglacial sample resolution for IBRD of 5–15 yr (Methods).

Sample analysis. IBRD was counted every centimetre on X-radiographs taken from 1-cm-thick slices that were cut out from the centre of each core segment and exposed to an X-ray system (Methods). Biogenic opal was determined using a combination of a traditional leaching method and newly introduced Fourier transform infrared spectroscopy.

Earth system modelling experiments. Coordinated Southern Ocean freshwater perturbation experiments were conducted with the Bern3D and LOVECLIM Earth system models of intermediate complexity and the coupled general circulation model COSMOS (Methods). The IBRD flux stack (Fig. 3a) is used as a Southern Ocean freshwater forcing time series for these models, assuming that 50% of the MWP-1A forcing originated from Antarctica, and attaining peak values of about 0.22 Sv at 14.67 kyr ago, coincident with the onset of the Bølling interstadial (14.64 kyr ago) and MWP-1A (14.65 kyr ago).

Online Content Any additional Methods, Extended Data display items and Source Data are available in the online version of the paper; references unique to these sections appear only in the online paper.

Received 5 July 2013; accepted 16 April 2014.
Published online 28 May 2014.

1. Clark, P. U. *et al.* The Last Glacial Maximum. *Science* **325,** 710–714 (2009).
2. Heroy, D. C. & Anderson, J. B. Radiocarbon constraints on Antarctic Peninsula ice sheet retreat following the Last Glacial Maximum. *Quat. Sci. Rev.* **26,** 3286–3297 (2007).
3. Mackintosh, A. *et al.* Retreat of the East Antarctic ice sheet during the last glacial termination. *Nature Geosci.* **4,** 195–202 (2011).
4. Weber, M. E. *et al.* Interhemispheric ice-sheet synchronicity during the Last Glacial Maximum. *Science* **334,** 1265–1269 (2011).
5. Bond, G. C. & Lotti, R. Iceberg discharges into the North Atlantic on millennial timescales during the last glaciation. *Science* **267,** 1005–1010 (1995).
6. Peltier, W. R. Global glacial isostasy and the surface of the ice-age Earth: the ICE-5G (VM2) model and GRACE. *Annu. Rev. Earth Planet. Sci.* **32,** 111–149 (2004).
7. Bentley, M. J. *et al.* Deglacial history of the West Antarctic Ice Sheet in the Weddell Sea embayment: constraints on past ice volume change. *Geology* **38,** 411–414 (2010).
8. Conway, H., Hall, B. L., Denton, G. H., Gades, A. M. & Waddington, E. D. Past and future grounding-line retreat of the West Antarctic ice sheet. *Science* **286,** 280–283 (1999).
9. Gladstone, R. M., Bigg, G. R. & Nicholls, K. W. Iceberg trajectory modeling and meltwater injection in the Southern Ocean. *J. Geophys. Res.* **106,** 19903–19915 (2001).
10. Silva, T. A. M., Bigg, G. R. & Nicholls, K. W. Contribution of giant icebergs to the Southern Ocean freshwater flux. *J. Geophys. Res.* **111,** C03004 (2006).
11. Stuart, K. M. & Long, D. G. Tracking large tabular icebergs using the SeaWinds Ku-band microwave scatterometer. *Deep Sea Res. II* **58,** 1285–1300 (2011).
12. Weber, M. E. *et al.* Dust transport from Patagonia to Antarctica—a new stratigraphic approach from the Scotia Sea and its implications for the last glacial cycle. *Quat. Sci. Rev.* **36,** 177–188 (2012).
13. EPICA Community Members. One-to-one coupling of glacial climate variability in Greenland and Antarctica. *Nature* **444,** 195–198 (2006).
14. Schmitt, J. *et al.* Carbon isotope constraints on the deglacial CO_2 rise from ice cores. *Science* **336,** 711–714 (2012).
15. Deschamps, P. *et al.* Ice-sheet collapse and sea-level rise at the Bølling warming 14,600 years ago. *Nature* **483,** 559–564 (2012).
16. Clark, P. U., Mitrovica, J. X., Milne, G. A. & Tamisiea, M. E. Sea-level fingerprinting as a direct test for the source of global meltwater pulse IA. *Science* **295,** 2438–2441 (2002).
17. Golledge, N. R., Fogwill, C. J., Mackintosh, A. N. & Buckley, K. M. Dynamics of the Last Glacial Maximum Antarctic ice-sheet and its response to ocean forcing. *Proc. Natl Acad. Sci. USA* **109,** 16052–16056 (2012).
18. Menviel, L., Timmermann, A., Timm, O. E. & Mouchet, A. Climate and biogeochemical response to a rapid melting of the West Antarctic ice sheet during interglacials and implications for future climate. *Paleoceanography* **25,** PA4231 (2010).
19. Bintanja, R., van Oldenborgh, G. J., Drijfhout, S. S., Wouters, B. & Katsman, C. A. Important role for ocean warming and increased ice-shelf melt in Antarctic sea-ice expansion. *Nature Geosci.* **6,** 376–379 (2013).
20. Peltier, W. R. & Fairbanks, R. G. Global glacial ice volume and Last Glacial Maximum duration from an extended Barbados sea level record. *Quat. Sci. Rev.* **25,** 3322–3337 (2006).

21. Bard, E., Hamelin, B. & Delanghe-Sabatier, D. Deglacial meltwater pulse 1B and Younger Dryas sea levels revisited with boreholes at Tahiti. *Science* **327,** 1235–1237 (2010).
22. Marshall, S. J. & Koutnik, M. R. Ice sheet action versus reaction: distinguishing between Heinrich events and Dansgaard-Oeschger cycles in the North Atlantic. *Paleoceanography* **21,** PA2021 (2006).
23. Pritchard, H. D. *et al.* Antarctic ice-sheet loss driven by basal melting of ice shelves. *Nature* **484,** 502–505 (2012).
24. Jenkins, A. *et al.* Observations beneath Pine Island Glacier in West Antarctica and implications for its retreat. *Nature Geosci.* **3,** 468–472 (2010).
25. Hellmer, H. H., Kauker, F., Timmermann, R., Determann, J. & Rae, J. Twenty-first-century warming of a large Antarctic ice-shelf cavity by a redirected coastal current. *Nature* **485,** 225–228 (2012).
26. Gladstone, R. M. *et al.* Calibrated prediction of Pine Island Glacier retreat during the 21st and 22nd centuries with a coupled flowline model. *Earth Planet. Sci. Lett.* **333–334,** 191–199 (2012).
27. Fischer, H. *et al.* Reconstruction of millennial changes in dust emission, transport and regional sea ice coverage using the deep EPICA ice cores from the Atlantic and Indian Ocean sector of Antarctica. *Earth Planet. Sci. Lett.* **260,** 340–354 (2007).
28. Anderson, R. F. *et al.* Wind-driven upwelling in the Southern Ocean and the deglacial rise in atmospheric CO_2. *Science* **323,** 1443–1448 (2009).
29. Sprenk, D. *et al.* Southern Ocean bioproductivity during the last glacial cycle—new decadal-scale insight from the Scotia Sea. *Geol. Soc. Lond. Spec. Publ.* **381,** 245–261 (2013).
30. NGRIP Members. High-resolution record of Northern Hemisphere climate extending into the last interglacial period. *Nature* **431,** 147–151 (2004).

Acknowledgements We acknowledge support from the Deutsche Forschungsgemeinschaft (DFG grant numbers We2039/7-1, Ri525/17-1 and Ku683/9-1 to M.E.W. and G.K.), the University of Cologne (to M.E.W.), the US NSF Antarctic Glaciology Program (grant numbers ANT-1043517 to P.U.C. and ANT-1341311 to A.T.), the US NSF Paleoclimatology Program and the Japan Agency for Marine-Earth Science and Technology (to A.T.), and Helmholtz funding through the Polar Regions and Coasts in the changing Earth System (PACES) programme (to X.Z., G.L. and G.K.). Our study was also part of the Southern Ocean Initiative of the International Marine Past Global Change Study (IMAGES) program. We thank W. F. Budd for comments on Antarctic ice-sheet dynamics, and M. Winstrup and S. Rasmussen for advice on comparing ice-core chronologies. Experiments with the Bern3D were performed in the Department of Climate and Environmental Physics, University of Bern, and with funding through the Oeschger Center for Climate Change.

Author Contributions M.E.W. conceived the idea for the study and, with P.U.C., wrote most of the manuscript. G.K. selected the core sites and provided geochemical data. A.T. oversaw the modelling contributions and helped write the manuscript. R.G. provided insight into iceberg routing and associated ice-sheet modelling. D.S. helped develop the age model and provided biogenic opal data. G.L. and X.Z. contributed results from the COSMOS model. L.M., M.O.C. and T.F. contributed results from Bern3D and LOVECLIM models. C.O. contributed uncertainty estimates on the different age models. All authors commented on the manuscript.

Author Information Further data are available at http://dx.doi.org/10.1594/PANGAEA.819646. Reprints and permissions information is available at www.nature.com/reprints. The authors declare no competing financial interests. Readers are welcome to comment on the online version of the paper.
Correspondence and requests for materials should be addressed to M.E.W. (michael.weber@uni-koeln.de).

METHODS

Material and sediment composition. If not tabulated here, data from this study are available at the Pangaea data library (http://dx.doi.org/10.1594/PANGAEA.819646). Sediment cores MD07-3133 (57° 26′ S, 43° 27′ W; 3,101 m water depth; 32.8 m core length) and MD07-3134 (59° 25′ S, 41° 28′ W; 3,663 m water depth; 58.2 m core length) were obtained from the northern end of Dove Basin and Pirie Bank, respectively, in the southern part of the central Scotia Sea (Fig. 1). Both sites are located well below the carbonate compensation depth, that is, the sediments are largely carbonate-free and consist primarily of biogenic opal and detrital material. The relative proportions of these two components depend on climate conditions (see below): warm periods are associated with homogenous, olive grey to yellowish diatomaceous oozes, whereas cold periods correspond to grey to blue-grey diatom-bearing mud, and climate transitions are associated with olive-grey diatomaceous mud[29].

Non-destructive measurements. We conducted a number of non-destructive measurements[12]. We determined magnetic susceptibility (kappa volume specific) with a Bartington coil sensor for whole-core and a point sensor for split-core measurements at 1-cm increments using a multi-sensor core logger[31]. We also measured the distribution of chemical elements using an AVAATECH X-ray fluorescence core scanner[32]. Results for Ca are given as peak area intensities determined in total counts per second. We performed the analysis using a sample spot of 1 cm × 1 cm in size at 1-cm increments[33].

We also used a Minolta spectrophotometer CM-2002 to measure L^*, a^* and b^* as well as RGB colour components[34] at 1-cm increments. RGB colour values were converted to R/G/B[35] and plotted with PanPlot (www.pangaea.de/software/PanPlot) to obtain visual colour logs (Fig. 2).

Biogenic opal determination. Biogenic opal was determined by several methods for sites MD07-3133 and MD07-3134 (ref. 29). We first analysed biogenic opal by leaching the sediment in 1 M NaOH solution[36] to obtain ground-truth information at critical transitions (MD07-3133: 1,655–2,785 cm, 112 samples; MD07-3134: 745–1,785 cm, 4,135–4,585 cm; 141 samples). We then implemented a new and fast technique that relies on this ground-truthing, called Fourier transform infrared spectroscopy[37], to obtain information on biogenic opal at 10-cm increments over the entire core lengths of sites MD07-3133 and MD07-3134 (316 and 575 samples, respectively). Note that biogenic opal flux rates in Fig. 3d are normalized for ^{230}Th to account for sediment focusing with the exception of MD07-3133, where no ^{230}Th data have been obtained so far[29].

Chronology. The low-resolution chronology of sites MD07-3133 and MD07-3134, which extend back to 36 kyr ago and 93 kyr ago, respectively, is described in ref. 12. It is based on several ground-truth data points associated with Marine Isotopic Stage boundaries, the correlation to rather massive layers rich in coarser-grained detritus[38], and the identification of the Laschamp event. The high-resolution chronology relies on dust–climate couplings between Southern Ocean sediment and the Antarctic EDML ice core[12]. The use of marine Fe records as a proxy for dust is a well-established approach reflecting coherent and synchronous changes in dust deposition across much of the Southern Ocean and the AIS, and has recently also been implemented to construct age models for records from the Atlantic[39] and the Pacific[40] sectors of the Southern Ocean to reconstruct Southern Hemisphere dust climate couplings during the Late Quaternary using Fe counts. In addition, a number of previous workers have identified a remarkable similarity in the structure of variability of magnetic susceptibility in cores from the Scotia Sea and the variability in dust records from Antarctic ice cores[41–43]. Pugh *et al.*[44] noted this similarity in magnetic susceptibility records from three cores in the Scotia Sea (that is, the same region as our records cover), and explicitly tested whether the magnetic susceptibility signal was synchronous with the EPICA ice-core dust record. They first established two independent age models for their cores from (1) biostratigraphy (variations in *Cycladophora davisiana* abundance tied to the LR04 time scale δ^{18}O global stack[45]) and (2) radiocarbon dating, and then compared those age models to one constructed by synchronizing their magnetic susceptibility records to the ice-core dust record. They concluded that these three independently derived age models are "mutually consistent over their common ranges" and that millennial-scale fluctuations in magnetic susceptibility and in Antarctic dust concentration were synchronous, supporting our strategy of tuning Scotia Sea magnetic susceptibility records to Antarctic ice-core dust records to develop an age model for our marine records[12].

Weber *et al.*[12] also noted a remarkable similarity in the structure of variability of Ca in the cores from the Scotia Sea and the variability in the non-sea-salt Ca records from Antarctic ice cores. Weber *et al.*[12] measured Ca by X-ray fluorescence which, because the Scotia Sea sites do not contain biogenic Ca, is the same proxy for dust as used in the ice cores (non-sea-salt Ca), and found that when Ca is tuned to non-sea-salt Ca (which is completely independent of the magnetic susceptibility tuning), the resulting correlation between the two is as strong as the correlation of magnetic susceptibility to non-sea-salt Ca, providing additional support for synchroneity, because both marine and ice-core Ca records are proxies for dust, with the most likely physical process being short-lived atmospheric transport.

Given these independent lines of evidence supporting synchronous changes, we tuned magnetic susceptibility and Ca in our cores to the non-sea-salt Ca flux record from the EDML ice core[27]. We used three statistical approaches to produce a tuned, high-resolution age model, evaluate its quality and provide error estimates[12]. Implementing dynamic time wrapping algorithms, for instance, helped to detect circularities by computing a time (depth) axis stretch and mapping two time series optimally by minimizing the cumulative distance without any pre-defined tie points. The resulting age–depth structure obtained from dynamic time wrapping was virtually identical to the one obtained by the tuning procedure, which served as independent verification of our final tuning with tie points.

Our deglacial age model is based primarily on five stratigraphic tie points (TP1 to TP5) that are shared between the records and reveal a detailed record for the period about 20–8 kyr ago over 10 m and 7 m core lengths for sites MD07-3133 and MD07-3134, respectively (Extended Data Fig. 1). The five tie points correspond to consistent breaks in slopes and characteristic and reproducible peaks in the records of magnetic susceptibility and Ca relative to non-sea-salt Ca. Our deglacial chronology also includes Fe, which shows the same characteristic trends and features as magnetic susceptibility and Ca, and which has been used to synchronize Southern Ocean marine sediment and Antarctic ice-core records[39,40]. TP1 (about 19 kyr ago) is one of many correlation points for the Last Glacial Maximum used in ref. 12. It marks the end of distinctly elevated values in magnetic susceptibility, Ca, Fe and non-sea-salt Ca towards the end of this phase. TP2 (about 17.6 kyr ago) is defined on the basis of a steep increase in slope in each of the records. A subsequent decrease in slope in each of the records is the basis for TP3 around 16.5 kyr ago. TP4 occurs another 1,800 years later with another distinct decrease in slope in each record around 14.7 kyr ago and a corresponding distinct peak in the non-sea-salt Ca and magnetic susceptibility records. TP5 is recorded in all archives as a distinct peak that occurred around 8.4 kyr ago.

In addition to these common tie points, site MD07-3134 and EDML share a dust peak at 12.85 kyr ago that is not preserved at site MD07-3133. Sites MD07-3133 and MD07-3134 share a weak dust peak at 11.42 kyr ago, which was taken as an additional age control for MD07-3133. This correlation is supported by the fact that colour component a^* (red–green variability) shows a distinct peak at 8.5–8.3 kyr ago at sites MD07-3133 and MD07-3134, which also serves as control point at both sites (Fig. 2c, d). This peak is replicated at 11.42 kyr ago (that is, at 19.00 m at site MD07-3133, and at 11.00 m at site MD07-3134).

Based on our age model, sedimentation rates in our cores are high, 0.2–1.2 m kyr^{-1} for site MD07-3134 (63 cm kyr^{-1} on average over the last 93 kyr) and 0.3–2.1 m kyr^{-1} for site MD07-3133 (92 cm kyr^{-1} on average over the last 36 kyr), translating into mass accumulation rates of 10–120 g cm^2 kyr^{-1} and 15–170 g cm^2 kyr^{-1}, and into sample resolutions of 8–50 yr and 5–33 yr (given a sample increment of 1 cm) for IBRD counting, respectively.

Considering the chronological limitations and problems that are associated with most Southern Ocean sediment archives, the age model of our two Scotia Sea sites has a high resolution and should be very accurate because the uncertainties associated with ^{14}C dating, such as reservoir age, are circumvented. Therefore, our expanded deglacial record of about 20–8 kyr ago (documented over 7 m and 10 m core length in sites MD07-3134 and MD07-3133, respectively) is chronologically better constrained than the deglacial signals that have been inferred from shallow-water archives around the Antarctic continent, such as at Mac Robertson Land[3], where inferred changes usually occur over a few centimetres in condensed, lithologically complex successions with partially reversed ^{14}C ages that have uncertain reservoir ages.

Age scale and AID uncertainty estimates. We use the EDML1/EDC3 age model that was developed in conjunction with the EDC age model[27] by incorporating ground-truth stratigraphic evidence, most importantly the correlation of regional volcanic ash layers. Based on this age model, three AIDs in the Scotia Sea correlate well with large-scale events: the peak of AID7 with the major retreat of the Weddell Sea part of the East AIS at 16.1 kyr ago[4], the peak of AID6 with MWP-1A around 14.7 kyr ago, and AID2 with MWP-1B at 11.3 kyr ago.

The original age scale EDML1/EDC3 relied on ash correlation to EDC[46,47]. The errors of this correlation are a couple of decades. For ages younger than 41 kyr ago, the EDML1/EDC3 age model is based on correlation of methane and ^{10}Be to the Greenland Ice Core Chronology 2005 (GICC05), which largely relies on layer counting[48]. The errors of GICC05 were also a couple of decades for the Holocene, and up to two centuries for the time around MWP-1A. Subsequent revision to the EDML age model[49] and the latest Antarctic-wide ice-core chronology[50], called AICC2012, tried to account for regional stratigraphic constraints and the need to adjust ages to achieve interhemispheric methane and ^{10}Be synchronization during deglaciation.

AICC2012 shows little to no difference to EDML1/EDC3 for most of the Holocene: that is, the timing of AID1 and AID2 are not affected. However, from about 8–18 kyr ago, AICC2012 becomes progressively older, with an age difference peaking

at about 550 yr at 18 kyr ago, and declining again to about 200 yr from the Last Glacial Maximum. For the time of MWP-1A, for instance, the age difference is almost 400 yr. This would increase the age of the tie point, which occurs right at the start of AIE6, from 14.8 kyr ago to almost 15.2 kyr ago, implying that the peak of AIE6 dates 15.1–14.7 kyr ago instead of 14.8–14.4 kyr ago. The entire AIE6 would hence be 15.2–14.2 kyr ago.

However, this age shift is only achieved at the expense of a significantly larger dating uncertainty than the original EDML1/EDC3 chronology. For the Holocene the uncertainty is around 200 yr (ref. 51). At about 12 kyr ago, it increases to almost 500 yr, and it reaches 1,000 yr by about 19 kyr ago. The original EDML1/EDC3 age scale, however, has much lower uncertainties. From approximately 10 kyr ago to 14 kyr ago, uncertainties increase from only a few decades to around 200 yr, respectively (Extended Data Fig. 2d), and then further increase to about 700 yr at around 18 kyr ago. One should note that, although AICC2012 is applied to all Antarctic ice cores, the only ground-truth correlation of EDML is established via volcanics to EDC.

Synchronization of the new West AIS ice core to EDML via layer counting between volcanic acidic horizons, which has not been included in AICC2012, indicates that AICC2012 is significantly too old for the pre-Holocene time (Winstrup, M., Vinther, B. M., Sigl, M., McConnell, J., Svensson, A. M. and Wegner, A., manuscript in preparation). For the depth around MWP-1A, for instance (about 800 m at EDML), this new chronology will again be closer to the timing of the original EDML1/EDC3 timescale. Also, the uncertainly will again be much lower, given the low counting error of annual bands between volcanic ashes.

Since the ageing of AICC2012 is only achieved at the expense of much higher uncertainties relative to the EDML1/EDC3 age scale, and all shifts are within the uncertainties of the different ice-core age models, we use the original EMDL1/EDC3 age model. We note also that its dating uncertainties are lower and that it has more ground-truth chronological constraints.

The original uncertainty estimates of the Scotia Sea sites[12] built upon a bootstrap algorithm that simulates possibly wrong tie points and therefore provides conservative error estimates. However, these uncertainty estimates do not include ice-core age uncertainties. We used the resulting dating errors (2σ) of the tie point correlation to calculate uncertainties for the start, end and duration of AIDs (Extended Data Fig. 2a). In addition, we considered the uncertainties in the EDML1 chronology[47] as well as the EDC3 chronology[46] when calculating the full uncertainties for the AIDs (Extended Data Fig. 2b). All uncertainties are incorporated into the absolute dating uncertainty (2σ error) of the AIDs (Extended Data Table 1). The bootstrap algorithm allows for the derivation of relative dating uncertainties for the AIDs. Since interpolation errors of nearby layers are highly correlated, these uncertainties are naturally smaller than the absolute dating uncertainties (Extended Data Fig. 2c). Hence, significantly more precise estimates can be made on the duration of and the distance between AIDs.

IBRD counting and conversion. We cut out 1-cm-thick, 10-cm-wide and 25-cm-long slices from the centre of each core section, placed them on plastic plates and exposed the slices to film-sensitive negatives for 3 min to 5 min using a HP 43855 X-ray system. The negatives were then scanned at 300 dpi (dots per inch) and analysed for the amount of IBRD using a 1-mm by 1-mm grid.

We counted all visible grains >1 mm in diameter per centimetre core depth[52] (that is, per 10 cm^3 volume) as an indicator for the content of IBRD (Extended Data Fig. 3). We distinguished between grains 1–2 mm and >2 mm in diameter. Also, to account for operator subjectivity in IBRD counts, three different individuals conducted independent counts, which were then averaged for Fig. 2c and d. For Fig. 2e, we stacked the results by re-sampling each data series at 10-yr increments, adding the individual counts from the two cores, and then dividing them by 2. For Fig. 2f, we converted the IBRD time series from sites MD07-3133 and MD07-1334 into flux rates, using the detailed age models[12], and, again, stacked the results. For Fig. 3b, we averaged the stacked IBRD flux rates into 500-yr slices.

The stacked IBRD flux-rate record indicates, on average, rather stable values with little multi-centennial variability of 0.01 grains $cm^2\ yr^{-1}$ for 25–21 kyr ago, and 0.015 grains $cm^2\ yr^{-1}$ for 8–0 kyr ago. We infer that these low values represent steady-state conditions, that is, the amount of iceberg calving off the Antarctic continent is balanced by accumulation on the ice sheet. During deglaciation, however, flux rates were distinctly above these low values, and 10–15 times higher during meltwater pulses. Even when averaged into 500-yr slices (grey histogram line, Fig. 3e), meltwater pulses show IBRD flux rates 4–7 times higher.

We note that icebergs usually lose the majority of their coarse-grained IBRD (pebbles to boulders) immediately after calving proximal to the AIS grounding lines. The largest IBRD reaching our distal core positions in Iceberg Alley is usually 1–3 mm in size and dispersed in a diatom-rich or clay-rich matrix (Extended Data Fig. 3). These particles embedded within icebergs can travel over long distances and argue against a strong regional bias in our IBRD data set.

On the relation of AIS mass loss, icebergs and IBRD. The majority of IBRD originates from bedrock, either directly (through scouring) or indirectly (through refreezing of sediment-laden water at the bed), and is entrained in the deeper part of a glacier. Where glaciers merge, medial moraines can cause IBRD to occur over a much greater thickness, sometimes even throughout the ice column (W. F. Budd, personal communication, 2013). Other processes internal to ice flow (for example, compressive flow) can also transport debris from the bed well up into the ice column. Only a small fraction will be delivered onto the ice surface, for example, by rock fall, or by wind transport in the case of finer grains.

In the floating ice shelves most IBRD near the base will melt out relatively close to the source[53,54], immediately in front of the grounding line. In ice shelves with high melt rates, the whole sediment-rich basal layer might ablate. However, in some ice shelves tributary glaciers can carry IBRD straight into a basal freeze-on zone, where they are protected from melting out by a layer of meteoric ice (for example, the west side of the Amery; see figures 6a and 9a of ref. 55). This process and the potential for localized IBRD throughout the ice column allow some IBRD to reach the front of large ice shelves.

The fact that we capture mostly small, englacial IBRD in Iceberg Alley indicates that the majority of the coarse-grained IBRD has been deposited before the icebergs reached the Scotia Sea sites. The fact that englacial material can travel long distances and will probably survive the counterclockwise journey around Antarctica (see below) within the Antarctic Coastal Current could therefore indicate that regional bias is not strong and no large nonlinearities exist between the amount of entrained IBRD detected in the Scotia Sea and the number of icebergs calving off the AIS.

Iceberg Alley today and during deglaciation. The term 'Iceberg Alley'[56] refers to the confluence zone where Antarctic icebergs merge[57] and exit the Weddell Sea to the north into the Scotia Sea[58]. Icebergs take several months to two years to complete their journey counterclockwise around Antarctica[9]. Although icebergs lose some mass in transit (through wave erosion, friction or collisions with sea ice), it is a rapid journey in cold waters. Therefore, melt rates remain low until the warmer Antarctic Circumpolar Current is reached, after which the icebergs ablate rapidly[59]. This is one of the reasons why the sites from Iceberg Alley should contain a circum-Antarctic-wide IBRD signal, although it is also reasonable to assume that the Weddell Sea part of the East AIS and the Antarctica Peninsula Ice Sheet provide more IBRD than more distal sources. This regional bias has been detected before in IBRD provenance studies[53,54], although deglaciations may involve different iceberg fluxes from various sources at different times as well as longer transport distances due to colder climates[60].

A substantial percentage of large icebergs reach Iceberg Alley through the Antarctic Coastal Current[11]. Some of the smaller icebergs (for example, in the vicinity of the Kerguelen plateau) may stray directly north due to topographic steering of ocean currents, but even the smaller icebergs mostly stay entrained in the Antarctic Coastal Current. Most icebergs calving from the Western AIS are not likely to reach Iceberg Alley through the Antarctic Coastal Current because there is a small northwards and clockwise escape route from the coastal drift (see arrow in Fig. 1; refs 9, 11). However, it is conceivable that these icebergs could also come through the Scotia Sea and affect the IBRD record of our sites.

Several factors indicate that the present-day iceberg routeing through Iceberg Alley would have remained largely the same during the last deglaciation. The Antarctic Divergence is the major driver of the ocean–atmospheric circulation in the Southern Ocean. It forces winds north of it to blow east and to feed clockwise into the Antarctic Circumpolar Current. South of the Antarctic Divergence, winds blow west and feed counterclockwise into the Antarctic Coastal Current around Antarctica. The Antarctic Circumpolar Current is constrained to flow south of the tip of South America at 56° S as it passes from the Pacific Ocean to the Atlantic Ocean, and its mean position therefore lies between 50° S and 55° S (ref. 61). The Antarctic Circumpolar Current and Antarctic Coastal Current will thus exist under different climates of the past[28,62], although specific fronts associated with them probably shifted north or south, depending on the state of the climate and its associated sea-ice coverage.

An additional factor that is important in routeing of icebergs discharged from the AIS is the Coriolis force, which depends on the rotation of the Earth and is therefore independent of the state of the climate. It causes all moving objects to be deflected to the left in the Southern Hemisphere. Thus, all icebergs calving from the AIS are forced to move counterclockwise and maintain a course parallel to the edge of the Antarctic continent. Moreover, the Coriolis force exerts a greater force on the larger icebergs[57], which contribute most of the AIS mass loss, and they thus largely remain entrained in the Antarctic Coastal Current (that is, sea ice does not have a large effect on altering the course of big icebergs); preferably smaller icebergs and crawlers would have escaped the Antarctic Coastal Current during times of thicker sea-ice coverage further away from the continent.

Finally, several studies[4,63] have reconstructed extensive coastal polynyas (areas of open water surrounded by sea ice) immediately in front of the AIS during colder periods when sea-ice coverage was dense further away from the continent. This further implies a vigorous Antarctic Coastal Current also during glacial and deglacial times. In summary, there are several lines of evidence that iceberg routeing through

Iceberg Alley operated in much the same way during deglaciation as is observed and modelled today.

We note that Kanfoush *et al.*[38] detected layers rich in coarser-grained detritus across the southern Atlantic, and named them SA0 (about 14–15 kyr ago) to SA6 (about 55 kyr ago). Whereas they interpreted these layers as IBRD and also inferred episodes of Antarctic ice-sheet instability from them, subsequent studies[64] demonstrated that the material was volcanic ash, most probably from the South Sandwich Islands, and concluded that the ash was deposited on sea ice, which then transported the material. In any event, the majority of Antarctic icebergs are entrained into the Antarctic Circumpolar Current in Iceberg Alley and melt long before these distal South Atlantic sites can be reached[57]. Moreover, the layers described by Kanfoush *et al.*[38] are distinct and massive, whereas our IBRD counts usually indicate small (1–3 mm in diameter) and dispersed grains embedded in a diatom- or clay-rich matrix. In addition, our IBRD records show no long-term correlation to the sea-salt Na record (Fig. 3f) of the EDML ice core, a proxy for sea ice. Accordingly, we are confident that the Scotia Sea IBRD counts indicate a source from icebergs with varying fluxes rather than a fallout from volcanic eruptions and transport by sea ice.

Deglacial meltwater sources. During deglaciation, specific parts of the AIS contributed to specific retreat events, that is, ice-sheet retreat probably did not occur contemporaneously across the entire AIS. The Weddell Sea sector of the East AIS probably contributed to AID8 (MWP-19KA; ref. 1) and AID7, with evidence that ice-sheet retreat occurred 19 kyr ago and 16 kyr ago, respectively[4]. Early deglaciation of the Antarctic Peninsula[65] and the Lambert glacier–Amery ice shelf system[66] may also have contributed icebergs to these events. In addition, the Pine Island glacier of the Amundsen Sea embayment retreated at 16.4 kyr ago[67], and may have contributed to AID7.

Evidence for widespread retreat 14–15 kyr ago comes from additional sectors of the East AIS, that is, Mac Robertson Land[3], as well as the Ross Sea sector of the West AIS[68,69] and the Antarctic Peninsula Ice Sheet[2,70], suggesting multiple sources for AID6 (MWP-1A). Such a change in the distribution of meltwater sources is supported by our freshwater experiments, which simulate increased subsurface temperature responses when sources are shifted from west to east during deglaciation. Subsequent retreat during AID2 (MWP-1B) is recorded at Wilkes Land, part of the East AIS[71]. Available terrestrial and shallow-marine records from the Ross Sea sector of the West AIS suggest retreat of the grounding line in the Ross Sea as having occurred either before[72] or after[8] AID1. Therefore, the specific sector of the AIS that contributed to this event remains unknown.

Ice-sheet/ocean feedbacks during AID6. To study the response of the Southern Hemisphere climate system to AID6-related iceberg surges, a series of coordinated transient climate modelling experiments is conducted with a hierarchy of climate models using time-varying Southern Ocean freshwater forcing (Extended Data Table 1). The freshwater forcing, which is evenly applied to the climate models in the Weddell and Ross seas, is a linearly scaled version of the IBRD flux stack of Fig. 3a. The scaling factor is determined by assuming that 50% of the maximum sea level rates during MWP-1A (40 mm yr^{-1})[15] originated from Antarctica. The corresponding peak freshwater forcing around Antarctica during AID6 reaches values of 0.22 Sv (Fig. 4). It should be noted here that the anomalous fresh water released from the Ross and Weddell seas is picked up by the Antarctic Circumpolar Current. This results in an efficient mixing of the freshwater around Antarctica, mimicking to some degree the effect of drifting icebergs[10] and their corresponding freshwater fluxes. The multi-model approach allows us to determine the robust features of the climate response to an Antarctic iceberg discharge 14.8–14.0 kyr ago (Fig. 3).

The following three climate models have been used: (1) The Bern3D model[73,74] is an intermediate-complexity model based on an energy-balance model for the atmosphere and a frictional geostrophic model for the ocean. Other components included in the Bern3D model, such as a carbon cycle and sediment component, are not considered here. The horizontal resolution adopted here is 5° by 10°. Atmospheric winds are prescribed at present-day values, thus inhibiting large-scale atmospheric circulation changes in response to the climate change. The freshwater forcing is applied to the Bern3D model under climate boundary conditions that represent the Last Glacial Maximum. (2) The global climate model LOVECLIM uses a simplified dynamical atmosphere coupled to an ocean general circulation model, and dynamic/thermodynamic sea-ice and diagnostic vegetation models. It has been used in a number of palaeoclimate studies focusing on the Southern Ocean[18,75,76]. Horizontal resolutions of the atmosphere and the ocean are 5.6° by 5.6° and 3° by 3°, respectively. Here the Southern Ocean freshwater forcing is applied to constant climate boundary conditions that represent the climate around 15 kyr ago[77]. These initial conditions were obtained from 5,000-yr-long spin-up experiments that use 15-kyr-ago greenhouse gas concentrations, orbital forcing and ice-sheet forcing. (3) COSMOS is a comprehensive coupled general circulation model including a land surface scheme and a dynamic sea-ice model. It has been extensively used to study various key palaeoclimate periods[78–80]. Horizontal resolutions of the atmosphere and the ocean are 3.75° and 3°, respectively. The freshwater forcing is applied under 15-kyr-ago boundary conditions. The initial state for the freshwater forcing experiment was obtained from a transient deglacial simulation varying CO_2 concentrations derived from EDC ice core[81] and orbital forcing.

Mimicking the effects of AID6, the applied Southern Hemisphere freshwater forcing causes widespread surface cooling in the Southern Hemisphere and an increase of Southern Ocean sea-ice area (Fig. 4), in accordance with the sea-salt Na^+ flux data from EPICA Dronning Maud Land (Fig. 3e). This cooling would contribute to establishing the Antarctic Cold Reversal and the bipolar seesaw response during the Bølling–Allerød. Moreover, the freshwater forcing generates a strong halocline, which inhibits formation of very cold Antarctic Bottom Water, which is then replaced by considerably warmer Circumpolar Deep Water (Fig. 4). Following previous studies[18,19], we hypothesize that the associated sub-surface warming at depths of 100–1,500 m can cause ice-shelf melting, grounding-line retreat, calving and subsequent release of more fresh water, all of which act as positive feedbacks.

31. Weber, M. E., Niessen, F., Kuhn, G. & Wiedicke, M. Calibration and application of marine sedimentary physical properties using a multi-sensor core logger. *Mar. Geol.* **136,** 151–172 (1997).
32. Jansen, J. H. F., Van der Gaast, S. J., Koster, B. & Vaars, A. J. CORTEX, a shipboard XRF-scanner for element analyses in split sediment cores. *Mar. Geol.* **151,** 143–153 (1998).
33. Richter, T. O. *et al.* The Avaatech XRF Core Scanner: technical description and applications to NE Atlantic sediments. *Geol. Soc. Lond. Spec. Publ.* **267,** 39–50 (2006).
34. Weber, M. E. Estimation of biogenic carbonate and opal by continuous non-destructive measurements in deep-sea sediments: application to the eastern Equatorial Pacific. *Deep Sea Res. I* **45,** 1955–1975 (1998).
35. Weber, M. E. *et al.* BMPix and PEAK tools: new methods for automated laminae recognition and counting—application to glacial varves from Antarctic marine sediment. *Geochem. Geophys. Geosyst.* **11,** 1–18 (2010).
36. Müller, P. J. & Schneider, R. An automated leaching method for the determination of opal in sediments and particulate matter. *Deep Sea Res. I* **40,** 425–444 (1993).
37. Rosén, P. *et al.* Fourier transform infrared spectroscopy, a new method for rapid determination of total organic and inorganic carbon and biogenic silica concentration in lake sediments. *J. Paleolimnol.* **43,** 247–259 (2010).
38. Kanfoush, S. I. *et al.* Millennial-scale instability of the Antarctic Ice Sheet during the last glaciation. *Science* **288,** 1815–1819 (2000).
39. Martínez-Garcia, A. *et al.* Southern Ocean dust-climate coupling over the past four million years. *Nature* **476,** 312–315 (2011).
40. Lamy, F. *et al.* Increased dust deposition in the Pacific Southern Ocean during glacial periods. *Science* **343,** 403–407 (2014).
41. Hofmann, A. *Kurzfristige Klimaschwankungen im Scotiameer und Ergebnisse zur Kalbungsgeschichte der Antarktis während der letzten 200 000 Jahre (Rapid climate oscillations in the Scotia Sea and results of the calving history of Antarctica during the last 200000 years)* PhD thesis (Univ. Bremen, 1999).
42. Diekmann, B. *et al.* Terrigenous sediment supply in the Scotia Sea (Southern Ocean): response to Late Quaternary ice dynamics in Patagonia and on the Antarctic Peninsula. *Palaeogeogr. Palaeoclimatol. Palaeoecol.* **162,** 357–387 (2000).
43. Yoon, H. I., Khim, B. K., Yoo, K. C., Bak, Y. S. & Lee, J. I. Late glacial to Holocene climatic and oceanographic record of sediment facies from the South Scotia Sea off the northern Antarctic Peninsula. *Deep Sea Res. II* **54,** 2367–2387 (2007).
44. Pugh, R. S., McCave, I. N., Hillenbrand, C. D. & Kuhn, G. Circum-Antarctic age modelling of Quaternary marine cores under the Antarctic Circumpolar Current: ice-core dust–magnetic correlation. *Earth Planet. Sci. Lett.* **284,** 113–123 (2009).
45. Lisiecki, L. E. & Raymo, M. E. A. Pliocene-Pleistocene stack of 57 globally distributed benthic δ18O records. *Paleoceanography* **20,** PA1003 (2005).
46. Parrenin, F. *et al.* The EDC3 chronology for the EPICA Dome C ice core. *Clim. Past* **3,** 485–497 (2007).
47. Ruth, U. *et al.* "EDML1": a chronology for the EPICA deep ice core from Dronning Maud Land, Antarctica, over the last 150 000 years. *Clim. Past* **3,** 475–484 (2007).
48. Rasmussen, S. O. *et al.* A new Greenland ice core chronology for the last glacial termination. *J. Geophys. Res.* **111,** D06102 (2006).
49. Lemieux-Dudon, B. d. *et al.* Consistent dating for Antarctic and Greenland ice cores. *Quat. Sci. Rev.* **29,** 8–20 (2010).
50. Veres, D. *et al.* The Antarctic ice core chronology (AICC2012): an optimized multi-parameter and multi-site dating approach for the last 120 thousand years. *Clim. Past Discuss.* **8,** 6011–6049 (2012).
51. Veres, D. *et al.* The Antarctic ice core chronology (AICC2012): an optimized multi-parameter and multi-site dating approach for the last 120 thousand years. *Clim. Past* **9,** 1733–1748 (2013).
52. Grobe, H. A simple method for the determination of ice-rafted debris in sediment cores. *Polarforschung* **57,** 123–126 (1987).
53. Roy, M., van de Flierdt, T., Hemming, S. R. & Goldstein, S. L. $^{40}Ar/^{39}Ar$ ages of hornblende grains and bulk Sm/Nd isotopes of circum-Antarctic glacio-marine sediments: implications for sediment provenance in the southern ocean. *Chem. Geol.* **244,** 507–519 (2007).
54. Pierce, E. L. *et al.* Characterizing the sediment provenance of East Antarctica's weak underbelly: the Aurora and Wilkes sub-glacial basins. *Paleoceanography* **26,** PA4217 (2011).
55. Galton-Fenzi, B. K., Hunter, J. R., Coleman, R., Marsland, S. J. & Warner, R. C. Modeling the basal melting and marine ice accretion of the Amery Ice Shelf. *J. Geophys. Res.* **117,** C09031 (2012).

56. Anderson, J. B. & Andrews, J. T. Radiocarbon constraints on ice sheet advance and retreat in the Weddell Sea, Antarctica. *Geology* **27,** 179–182 (1999).
57. Schodlok, M. P., Hellmer, H. H., Rohardt, G. & Fahrbach, E. Weddell Sea iceberg drift: five years of observations. *J. Geophys. Res.* **111,** C06018 (2006).
58. Pudsey, C. J. & Howe, J. A. Quaternary history of the Antarctic Circumpolar Current: evidence from the Scotia Sea. *Mar. Geol.* **148,** 83–112 (1998).
59. Jacka, T. H. & Giles, A. B. Antarctic iceberg distribution and dissolution from ship-based observations. *J. Glaciol.* **53,** 341–356 (2007).
60. Williams, T. *et al.* Evidence for iceberg armadas from East Antarctica in the Southern Ocean during the late Miocene and early Pliocene. *Earth Planet. Sci. Lett.* **290,** 351–361 (2010).
61. Toggweiler, J. R. & Russell, J. Ocean circulation in a warming climate. *Nature* **451,** 286–288 (2008).
62. Toggweiler, J. R. & Lea, D. W. Temperature differences between the hemispheres and ice age climate variability. *Paleoceanography* **25,** PA2212 (2010).
63. Smith, J. A., Hillenbrand, C.-D., Pudsey, C. J., Allen, C. S. & Graham, A. G. C. The presence of polynyas in the Weddell Sea during the Last Glacial Period with implications for the reconstruction of sea-ice limits and ice sheet history. *Earth Planet. Sci. Lett.* **296,** 287–298 (2010).
64. Nielsen, S. H. H., Hodell, D. A., Kamenov, G., Guilderson, T. & Perfit, M. R. Origin and significance of ice-rafted detritus in the Atlantic sector of the Southern Ocean. *Geochem. Geophys. Geosyst.* **8,** 1–23 (2007).
65. Nakada, M. *et al.* Late Pleistocene and Holocene melting history of the Antarctic ice sheet derived from sea-level variations. *Mar. Geol.* **167,** 85–103 (2000).
66. White, D. A., Fink, D. & Gore, D. B. Cosmogenic nuclide evidence for enhanced sensitivity of an East Antarctic ice stream to change during the last deglaciation. *Geology* **39,** 23–26 (2011).
67. Kirshner, A. E. *et al.* Post-LGM deglaciation in Pine Island Bay, West Antarctica. *Quat. Sci. Rev.* **38,** 11–26 (2012).
68. Hall, B. L. & Denton, G. H. Radiocarbon chronology of Ross Sea drift, Eastern Taylor Valley, Antarctica: evidence for a grounded ice sheet in the Ross Sea at the Last Glacial Maximum. *Geogr. Ann.* **82,** 305–336 (2000).
69. Price, S. F., Conway, H. & Waddington, E. D. Evidence for late Pleistocene thinning of Siple Dome, West Antarctica. *J. Geophys. Res.* **112,** F03021 (2007).
70. Simms, A. R., Milliken, K. T., Anderson, J. B. & Wellner, J. S. The marine record of deglaciation of the South Shetland Islands, Antarctica since the Last Glacial Maximum. *Quat. Sci. Rev.* **30,** 1583–1601 (2011).
71. Leventer, A. *et al.* Marine sediment record from the East Antarctic margin reveals dynamics of ice sheet recession. *Geol. Soc. Am. Today* **16,** 4–10 (2006).
72. McKay, R. M. *et al.* Retreat history of the Ross Ice Sheet (Shelf) since the Last Glacial Maximum from deep-basin sediment cores around Ross Island. *Palaeogeogr. Palaeoclimatol. Palaeoecol.* **260,** 245–261 (2008).
73. Menviel, L. & Joos, F. Toward explaining the Holocene carbon dioxide and carbon isotope records: results from transient ocean carbon cycle-climate simulations. *Paleoceanography* **27,** PA1207 (2012).
74. Ritz, S. P., Stocker, T. F. & Joos, F. A coupled dynamical ocean–energy balance atmosphere model for paleoclimate studies. *J. Clim.* **24,** 349–375 (2011).
75. Menviel, L., Timmermann, A., Mouchet, A. & Timm, O. Climate and marine carbon cycle response to changes in the strength of the Southern Hemispheric westerlies. *Paleoceanography* **23,** PA4201 (2008).
76. Timmermann, A., Timm, O., Stott, L. & Menviel, L. The roles of CO_2 and orbital forcing in driving Southern Hemispheric temperature variations during the last 21 000 Yr. *J. Clim.* **22,** 1626–1640 (2009).
77. Timm, O., Timmermann, A., Abe-Ouchi, A., Saito, F. & Segawa, T. On the definition of seasons in paleoclimate simulations with orbital forcing. *Paleoceanography* **23,** PA2221 (2008).
78. Knorr, G., Butzin, M., Micheels, A. & Lohmann, G. A warm Miocene climate at low atmospheric CO_2 levels. *Geophys. Res. Lett.* **38,** L20701 (2011).
79. Zhang, X., Lohmann, G., Knorr, G. & Xu, X. Different ocean states and transient characteristics in Last Glacial Maximum simulations and implications for deglaciation. *Clim. Past* **9,** 2319–2333 (2013).
80. Wei, W., Lohmann, G. & Dima, M. Distinct modes of internal variability in the global meridional overturning circulation associated with the Southern Hemisphere westerly winds. *J. Phys. Oceanogr.* **42,** 785–801 (2012).
81. Lourantou, A. *et al.* Constraint of the CO_2 rise by new atmospheric carbon isotopic measurements during the last deglaciation. *Glob. Biogeochem. Cycles* **24,** GB2015 (2010).

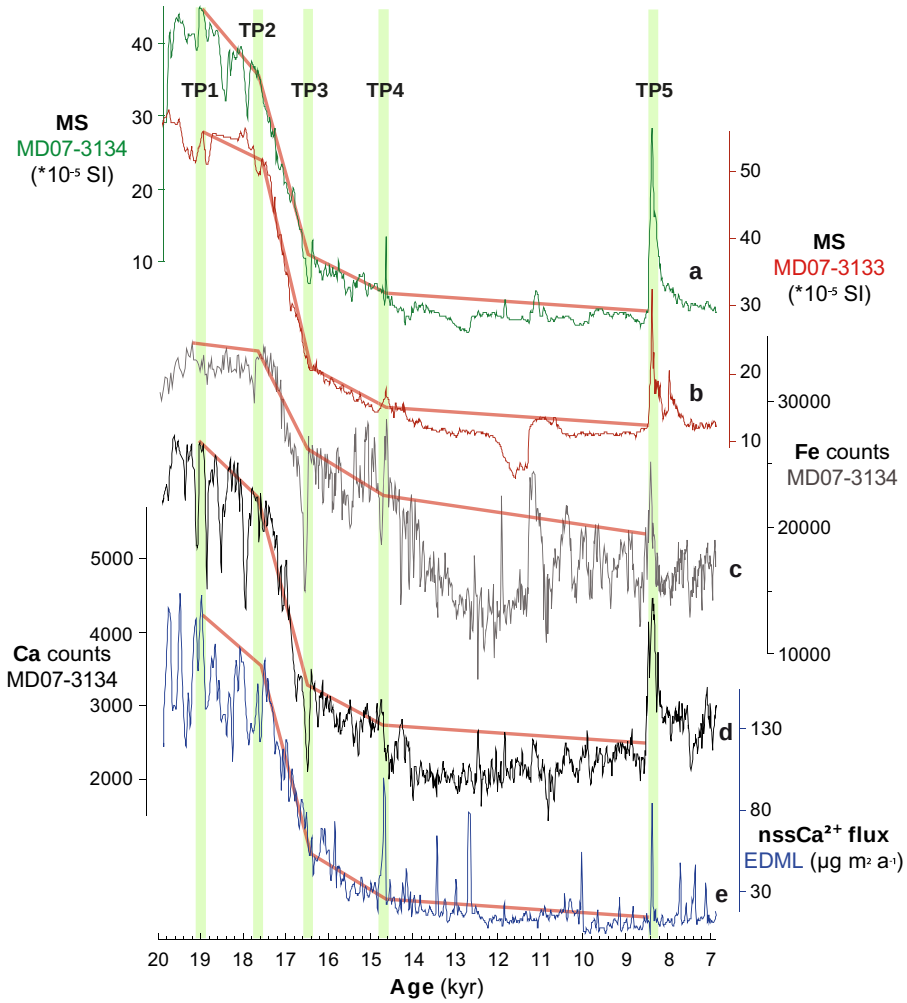

Extended Data Figure 1 | Deglacial dust chronology. Five common tie points (TP1 to TP5, indicated by green vertical bands) depict consistent changes in slope and reproducible lows and highs between magnetic susceptibility (**a**, **b**), Fe (**c**) and Ca (**d**) records of deep-sea sites MD07-31333 and MD07-313412, and the non-sea-salt Ca record (**e**) of the EDML ice core[27].

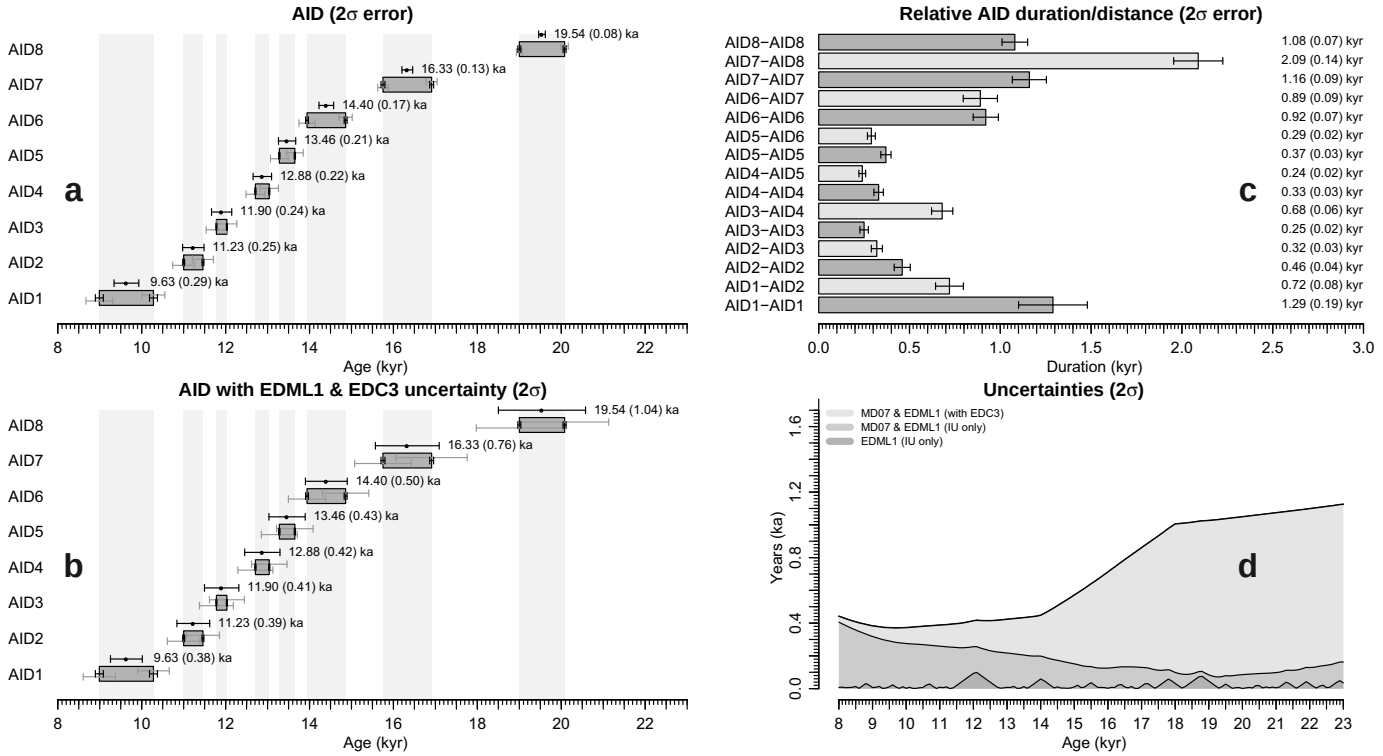

Extended Data Figure 2 | Uncertainty estimates for AIDs. Conservative error estimates (2σ) rely on bootstrapping of different age models and projecting them on to AIDs. **a**, Errors of the MD age model[12] based on tie point correlation only. Black dots depict the centre of the AID and its absolute uncertainty range. Black error bars at the boxes mark the relative uncertainty with respect to the centre. Grey error bars show the absolute uncertainty of the beginning and end of each AID. **b**, Errors including the EDML1 (ref. 47), and EDC3 (ref. 46) uncertainties. **c**, Relative duration of AIDs and related uncertainties. **d**, Error propagation of the three different age scales through the last deglaciation. IU is interpolation uncertainty. Note that uncertainties are highly correlated for nearby ages. Accounting for this correlation, the duration of each AID as well as the time between two AIDs is significantly more accurate than its absolute age uncertainty.

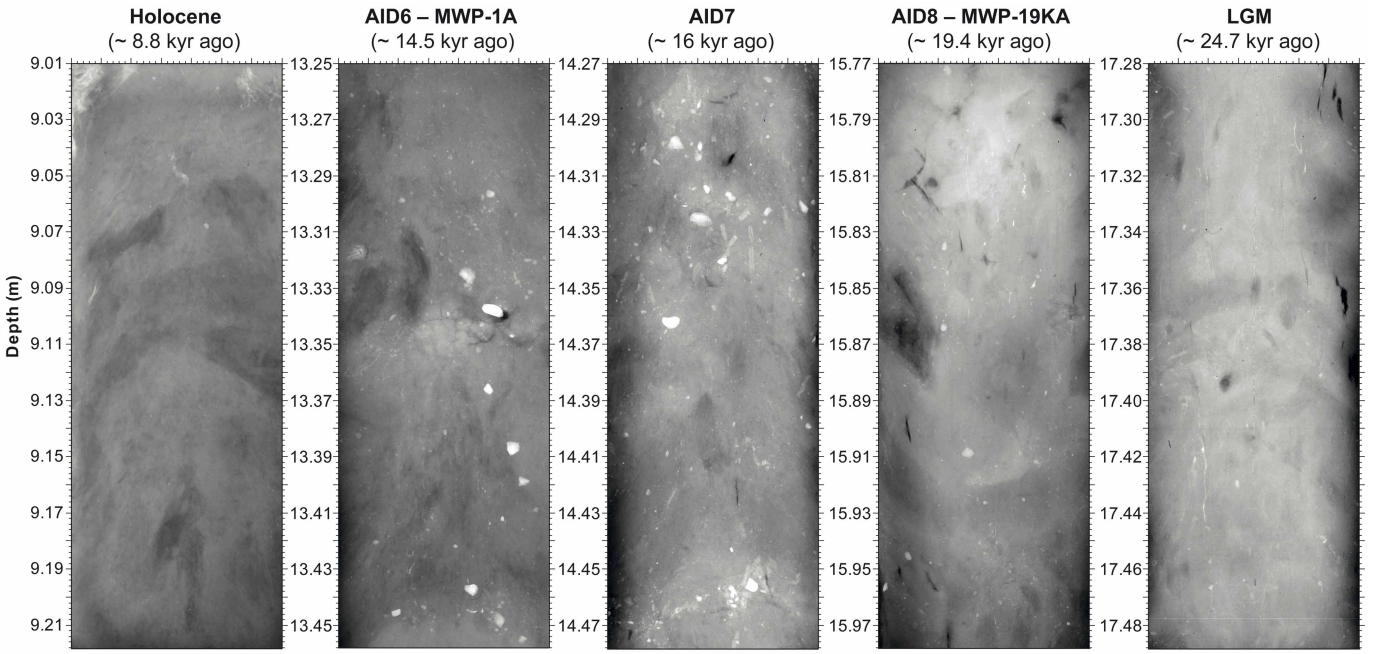

Extended Data Figure 3 | X-radiograph images from Scotia Sea Site MD07-3134. IBRD (bright dropstones) are embedded in a matrix-supported diatomaceous mud. Low IBRD contents are documented for the Last Glacial Maximum (LGM, ~24.7 kyr ago) and the Holocene (~8.8 kyr ago), whereas higher numbers indicate enhanced iceberg routeing through Iceberg Alley during three distinct deglaciation phases (centre panels): AID8 (MWP-19KA), AID7 and AID6 (MWP-1A).

Extended Data Table 1 | Uncertainty estimates

AID No.	Top (kyr)	Error (2σ)	Centre (kyr)	Error (2σ)	Bottom (kyr)	Error (2σ)
AID1	8.99	(0.32, 0.38)	9.63	(0.29, 0.38)	10.28	(0.27, 0.38)
AID2	11.00	(0.26, 0.39)	11.23	(0.25, 0.39)	11.46	(0.25, 0.39)
AID3	11.78	(0.24, 0.40)	11.90	(0.24, 0.41)	12.03	(0.24, 0.42)
AID4	12.71	(0.22, 0.42)	12.88	(0.22, 0.42)	13.04	(0.22, 0.42)
AID5	13.28	(0.21, 0.43)	13.46	(0.21, 0.43)	13.65	(0.20, 0.44)
AID6	13.94	(0.19, 0.44)	14.40	(0.17, 0.50)	14.86	(0.16, 0.55)
AID7	15.75	(0.13, 0.67)	16.33	(0.13, 0.76)	16.91	(0.13, 0.85)
AID8	19.00	(0.07, 1.03)	19.54	(0.08, 1.04)	20.08	(0.09, 1.05)

Top, bottom, and centre of deglacial AID1 to AID8, as well as absolute dating uncertainties in terms of the 2σ error (parenthesis). The first uncertainty relates to the MD07 chronology only[12], the one below to the overall uncertainty including the EDML1 (ref. 47) and EDC3 (ref. 46) chronology.